


EFFECT OF TRANSITION METALS ADDITION ON THE MICROSTRUCTURE AND INCIPIENT MELTING OF 354-BASED ALLOYS

L. Alyaldin, A. M. Samuel , and F. H. Samuel

Département des Sciences appliquées, Université du Québec à Chicoutimi, Chicoutimi, QC, Canada

H. W. Doty

General Motors Materials Engineering, Pontiac, MI, USA

S. Valtierra

Nemak, S.A, Garza Garcia, NL, Mexico

Copyright © 2019 American Foundry Society
<https://doi.org/10.1007/s40962-019-00331-2>

Abstract

Thermal analysis of various 354 alloy melts was carried out to determine the sequence of reactions and phases formed during solidification under close-to-equilibrium cooling conditions. The main reactions observed comprised formation of the α -Al dendritic network at 598 °C followed by precipitation of the Al–Si eutectic and post-eutectic β -Al₅FeSi phase at 560 °C; Mg₂Si phase and transformation of the β -phase into π -Al₈Mg₃FeSi₆ phase at 540 °C and 525 °C; and lastly, precipitation of Al₂Cu and Q-Al₃Mg₈-Cu₂Si₆ at 498 °C and 488 °C. As a result of the low solidification rate of the thermal analysis castings, all Zr-containing alloys are located in the L + Al₃Zr region of the Al–Zr phase diagram during the melting stage. Three main reactions are detected with the addition of Ni, i.e., the

formation of AlFeNi, AlCuNi and AlSiNiZr phases. Larger sizes of AlFeNi and AlCuNi phase particles were observed in higher Ni content alloys of 3.6 wt%. Mn addition helps in reducing the detrimental effects of the β -iron phase by replacing it with the less-detrimental Chinese script α -Al₁₅(Fe,Mn)₃Si₂ phase and sludge particles. With the use of the multi-step solution treatment—involving higher solution temperatures and longer durations, an increased amount of incipient melting is likely to occur.

Keywords: aluminum alloys, thermal analysis, heat treatment, microstructure, incipient melting

Introduction

Alloying elements are usually added to Al–Si cast alloys in order to improve microstructure features and thus improve mechanical properties. Nickel (Ni) and zirconium (Zr) are used as minor additions to increase high-temperature strength in aluminum alloys due to the formation of the L1₂-type Al₃Zr dispersoids or Al₃Ni, which are more stable at higher temperatures than the precipitates existing in cast aluminum alloys such as Al₂Cu and Mg₂Si.¹ Manganese (Mn) is used to neutralize the effect of iron (Fe) and to modify the morphology and type of intermetallic phases formed.²

Zirconium is usually added to aluminum alloys in small amounts ranging from 0.1 to 0.25%. Precipitation of the Al₃Zr dispersoid particles is finer than those of Mn aluminides (10–100 nm).³ Nickel is added to Al–Cu and Al–Si alloys to improve hardness and strength at elevated temperatures and to reduce the coefficient of thermal expansion, as there is an increasing demand for Al–Si cast alloys with better performance concerning yield and tensile strength at elevated temperatures up to 250 °C.^{4,5} In fact, the addition of alloying elements such as Cu and Ni is an effective and practical way to improve the mechanical properties, especially in relation to the performance of piston alloys which are subjected to high-temperature service conditions.^{6,7}

It is common practice to add Ti to Al–Si foundry alloys because of its potential grain refining effect.^{8–10} Sigworth and Kuhn¹¹ have reported that the grain refining effect of titanium is enhanced if boron is present in the melt or if the Ti is added in the form of an Al–Ti–B master alloy containing boron and titanium, largely combined as TiB₂, which act as excellent nuclei for the α -Al phase. Titanium diboride has almost no solubility in liquid aluminum; thus, TiB₂ particles produce good refinement at small addition levels.

Alloys such as the 354 (Al–9 wt% Si–1.8 wt% Cu–0.5 wt% Mg) alloys show a greater response to heat treatment as a result of the presence of both Mg and Cu. These alloy types display excellent strength values at both low and high temperatures. Additions of Zr, Ni, Mn and Sc would be expected to maintain the performance of these alloys at still higher temperatures.

The current study was carried out to analyze the effects of Ni, Mn, Zr additions on the behavior of cast as well as solution heat-treated aluminum alloy 354 (Al–9%Si–1.8%Cu–0.5%Mg). The evolution of the microstructural features with the addition of the above elements was investigated. Based on this approach, the principal objective of this study was to examine the main microstructural features observed in the alloys, such as phases, intermetallics and precipitates, together with their identifying characteristics and evolution during controlled exposure at different temperatures and times. This study forms part of the Master's thesis of L. Alyaldin where the tensile properties at room and high temperature of these alloys were also investigated¹² and an extension of the work carried out by Garza-Elizondo et al.¹³

Experimental Procedure

The alloy ingots of the base 354 alloy were melted in a 120-kg capacity SiC crucible, using an electrical resistance furnace. The melting temperature was maintained at 750 ± 5 °C. Additions of Ni, Zr, Mn were carried out using Al–20 wt% Ni, Al–20 wt% Zr, Al–25 wt% Mn master alloys, respectively. The nominal additions were 2 and 4 wt% Ni, 0.25 wt% Zr and 0.75 wt% Mn. The melts were degassed for ~ 15 –20 min with a rotary graphite

impeller rotating at ~ 130 rpm, using pure dry argon. The melts were grain refined and modified using Al–5%Ti–1%B and Al–10%Sr master alloys, respectively, to obtain levels of 0.15% Ti and about 200 ppm Sr in the melt followed by degassing for a few minutes to ensure melt homogeneity and to minimize Sr oxidation. Following this, the melt was carefully skimmed to remove oxide layers from the surface. The hydrogen content was monitored using AlScanTM (0.12–0.15 ml/100 g Al). The melt was poured into an ASTM B-108 permanent mold preheated at 450 °C to drive out moisture, in order to prepare the tensile test bars. The chemical analysis was carried out using a Spectrolab JrCCD Spark Analyzer. Table 1 lists the actual chemical compositions of the various alloys used in the present work and their corresponding codes. The values in bold highlight the additions made in each case. Figure 1a shows an example of the size and distribution of TiB₂ in the solidified tensile bar of alloy R.

Tensile test bars of alloys R, S, T, U, V were subjected to solution heat treatment (SHT) under two different conditions, as follows.

- SHT 1: Solution heat treatment at 495 °C/5 h, and
- SHT 2: Multi-step solution heat treatment: 495 °C/5 h, then 515 °C/2 h, then 530 °C/2 h.

In order to obtain the cooling curves and to identify the main reactions and corresponding temperatures occurring during the solidification of the 354 alloys produced, thermal analysis of the alloy melts was carried out. Ingots of the as-received commercial 354 alloy were cut into smaller pieces, cleaned and then dried to prepare the required alloys. The melting process was carried out in a cylindrical graphite crucible of 2-kg capacity, using an electrical resistance furnace. The melting temperature was maintained at 780 °C, while the alloys were grain-refined by adding 0.2%Ti as Al–5%Ti–1%B master alloy in rod form and modified by Sr in the form of an Al–10%Sr master alloy (see Table 1).

Nickel, zirconium, and manganese were added to the melts in the form of Al–20 wt% Ni, Al–20 wt% Zr and Al–25 wt% Mn master alloys, respectively, as was the case with the casting of the tensile test samples. For determining the reactions taking place during solidification, part of the molten

Table 1. Chemical Composition of the Alloys Used in This Study and Their Codes

Alloy code	Si	Fe	Cu	Mn	Mg	Ti	Sr	Ni	Zr	Al
R	8.70	0.20	1.95	0.02	0.73	0.15	0.0143	~	0.23	Bal.
S	9.08	0.19	1.88	0.02	0.83	0.16	0.0170	1.8	0.21	Bal.
T	8.92	0.18	1.88	0.02	0.78	0.15	0.0175	3.6	0.18	Bal.
U	8.85	0.20	1.88	0.71	0.76	0.14	0.0168	~	0.19	Bal.
V	8.85	0.20	1.88	0.68	0.76	0.14	0.0168	1.7	0.21	Bal.

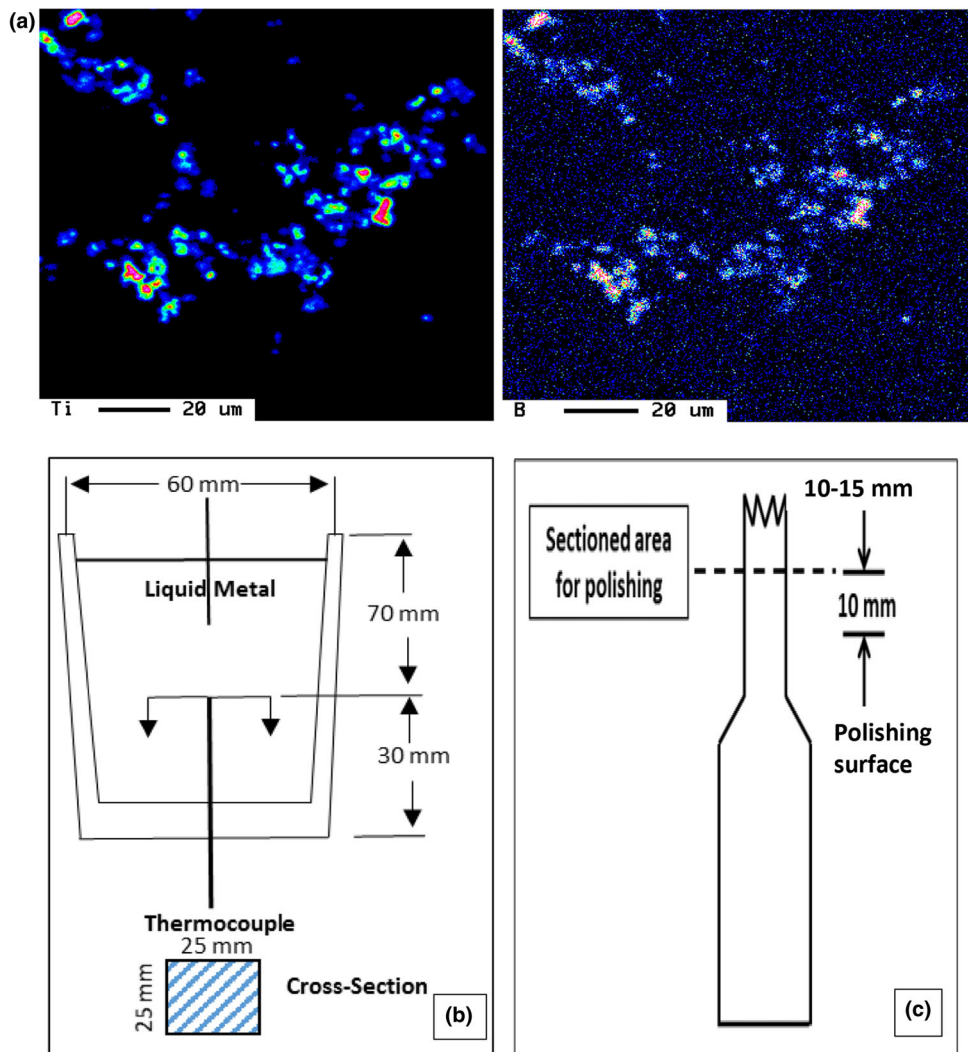


Figure 1. (a) X-ray images showing distribution of Ti and B in alloy R. Schematic drawings showing (b) the graphite mold used for thermal analysis, and (c) sample sectioned for metallography from tensile-tested bar.

metal was also poured into an 800 g capacity graphite mold preheated to 650 °C to obtain near-equilibrium solidification conditions at a cooling rate of 0.35 °C s⁻¹. A high sensitivity type-K (chromel–alumel) thermocouple, insulated using a double-holed ceramic tube, was attached to the center of the graphite mold. The temperature–time data were collected using a high-speed data acquisition system linked to a computer system that recorded the data every 0.1 s—Figure 1b. From these data, the cooling curves and the corresponding first derivative curves for a number of selected alloys were plotted to identify the main reactions occurring during solidification with the corresponding temperatures; the various phases, which constituted the microstructure of each alloy, were expected to be revealed as well. In support of the findings obtained from thermal analysis, DSC runs were carried out on alloys R through V at a solidification rate of 10 °C/min. Samples for metallography (about 10 mm thick) were sectioned from the tensile-tested bars of selected conditions of the alloys studied, approximately 10–15 mm below the fracture

surface, as shown in Figure 1c, the polishing surface of the sample being the side farther away from the fracture surface to avoid the deformation zone. The samples were individually mounted and then subjected to grinding and polishing procedures to produce a mirror-like surface. The mounting of the samples in bakelite was carried out using a Struers LaboPress-3 machine, while the grinding and polishing procedures were carried out using a TegraForce-5 machine. The microstructures of the polished sample surfaces were examined using an Olympus PMG3 optical microscope linked to a Clemex Vision P image analysis system.

Results and Discussion

DSC Runs

Figure 2 displays the DSC runs obtained from the five alloys during solidification at a rate of 10 C/min.

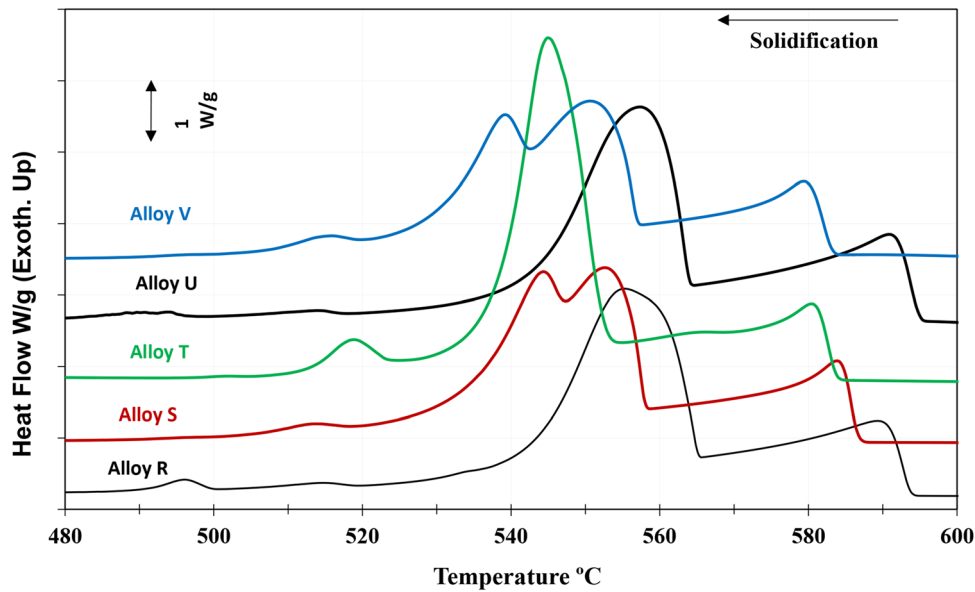


Figure 2. DSC runs of alloys R through V during solidification at 10 °C/min.

Table 2. Suggested Main Reactions Occurring During Solidification of 354-Type Alloys¹⁴

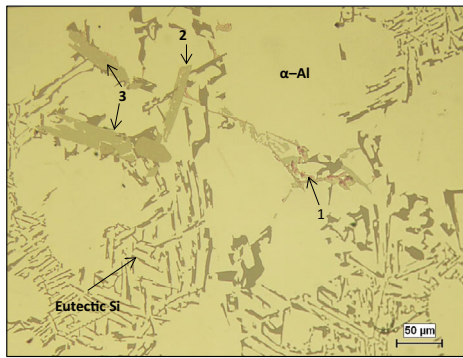
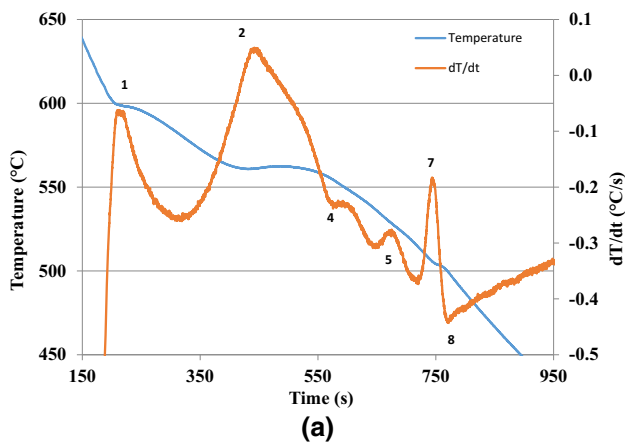
Reaction	Suggested temperature range (°C)	Suggested precipitated phase
1. Al	600–597	Formation of α -Al dendritic network
2. Al–Si, β -Fe and α -Fe	560–558	Development of Al–Si eutectic phase Precipitation of post-eutectic β -Al ₅ FeSi phase In case of presence of Mn, precipitation of α -Al ₁₅ (Mn,Fe) ₃ Si ₂ phase
3. Fe–Ni	555–556	Precipitation of Al ₉ FeNi phase
4. Mg–Si	540–538	Precipitation of Mg ₂ Si phase
5. π -phase	525–523	Transformation of β -Al ₅ FeSi phase to π -Al ₈ Mg ₃ FeSi ₆ phase
6. Al–Cu–Ni	523–520	Precipitation of Al ₃ CuNi phase
7. Al–Cu	500–496	Formation of eutectic Al–Al ₂ Cu phase
8. Q-phase	485–489	Formation of Q-Al ₅ Mg ₈ Cu ₂ Si ₆ phase

Based on the peaks presented in Figure 1, the following observations may be noted.

- All alloys are having more or less the same liquidus temperature except for alloy U containing 0.75% Mn, which may be attributed to precipitation of sludge followed by the α -Fe phase.
- Addition of 0.75% Mn to alloy R, i.e., alloy U produces no noticeable change in the Al–Si eutectic temperature.
- Alloys containing 2% Ni (S and V) revealed an explicit peak in the temperature range (543–539 °C) with a faint peak at 514 °C, corresponding to Ni-rich phases.
- Alloy T is characterized by the absence of both Al₂Cu phase and the phase precipitates following the Al–Si reaction. Instead, a significantly strong peak is seen at 519 °C.
- With the increase in added amount of Ni, the Al–Si eutectic temperature decreased from 556 °C (0%Ni) to 551 °C (2%Ni), to 545 °C (4%Ni), i.e., 2.7 °C per 1% Ni.

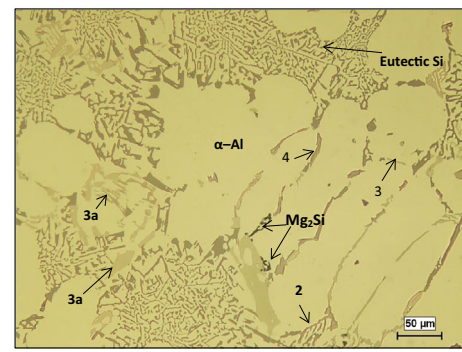
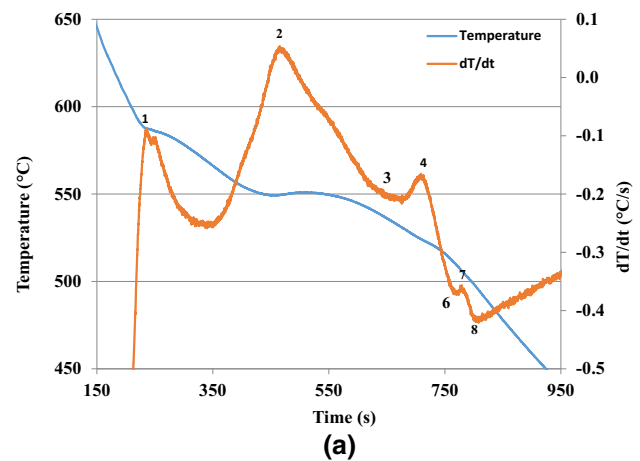
Thermal Analysis (Solidification Rate ~ 0.35 °C/s)

From the thermal analysis data, the solidification curve and the first derivative curve were plotted for each alloy condition. The reactions expected to occur (marked 1 through 8 in the thermal analysis plots) are listed in Table 2 and



(b)

Figure 3. (a) Temperature–time plot and first derivative obtained from the thermal analysis of alloy R (354 + 0.23%Zr). (b) Optical microstructure of R (354 + 0.23%Zr) alloy sample obtained from the thermal analysis casting (cooling rate 0.35 °C/s), showing the different phases present in the alloy: 1—Al₂Cu; 2—AlMgCuSi; 3—AlZrTi.



(b)

Figure 4. (a) Temperature–time plot and first derivative obtained from the thermal analysis of alloy S (354 + 0.21%Zr + 1.8%Ni). (b) Optical microstructure of alloy S (354 + 0.21%Zr + 1.8%Ni) sample obtained from the corresponding thermal analysis casting (cooling rate 0.35 °C/s), showing the different phases present in the alloy: 2—AlCuNi; 3—AlNiFe; 3a—AlSiNiZrFe; 4—Al₂Cu.

Table 3. Summary of Reactions in Alloy R

Reaction #	Proposed reaction	Temperature (°C)
1	Development of α-Al network	598
2	Precipitation of the Al–Si eutectic	560
4	Precipitation of the Mg ₂ Si phase	540
5	Partial transformation of β-phase into π-Al ₈ Mg ₃ FeSi ₆ phase	525
7	Solidification of Al–Cu eutectic	498
8	Solidification of Q-Al ₅ Mg ₈ Cu ₂ Si ₆	488

were identified with reference to the atlas of Backerud et al.¹⁴ on the solidification of aluminum foundry alloys. The four main reactions observed correspond to the formation of the α-Al dendrite network (peak 1), followed by the precipitation of the Al–Si eutectic (peak 2), and the precipitation of the copper phases (peaks 6 through 8).

Samuel et al.¹⁵ proposed the mechanism involved in Al₂Cu precipitation as follows:

- during the first stages of solidification, the formation of the α-Al dendritic network is associated with Si and Cu in the melt, ahead of the progressing dendrites;
- when the solidification temperature approaches the eutectic temperature, Si particles solidify from the melt, leading to a local concentration of Cu in the remaining areas.

The Al₂Cu phase was more often observed to solidify in the block like form rather than in the fine eutectic form. Magnesium also led to the formation of the Al₅Mg₈Cu₂Si₆ and Mg₂Si phases, and to the splitting of the copper phase formation temperature range into two explicit peaks representing the solidification of Al₂Cu and Al₅Mg₈Cu₂Si₆ microconstituents.

Alloy R (354 + 0.23%Zr)

Figure 3a shows the solidification curve and its first derivative obtained from the thermal analysis of alloy R, i.e., 354 alloy with 0.23 wt% Zr addition. Several reactions take place during the course of solidification, as marked by the different numbers on the first derivative curve. These numbers correspond to the reactions listed in Tables 2 and 3. In Zr-containing alloys, Al_3Zr particles may appear in various forms as square, rectangular or rounded. As a result of the low cooling rate of the thermal analysis castings, and a Zr content of 0.23 wt%, all Zr-containing alloys are located in the L + Al_3Zr region of the Al–Zr phase diagram during the melting stage. Thus, the coarse Al_3Zr particles may not dissolve in the melt and provide nucleation sites for the formation of Zr- and Ti-intermetallics from the melt during solidification.^{15–17} Apart from the α -Al dendrites and the eutectic Si particles observed in the interdendritic regions, $(\text{Al,Si})_3(\text{Ti,Zr})$ phase particles may also be observed in the optical micrograph of the corresponding sample, as shown in Figure 3b.

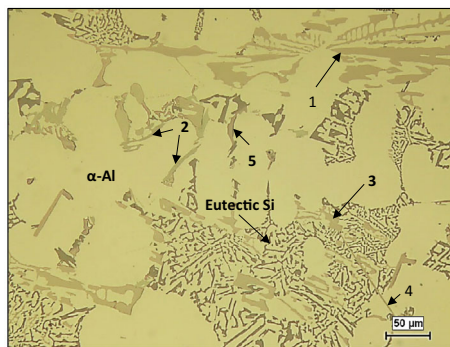
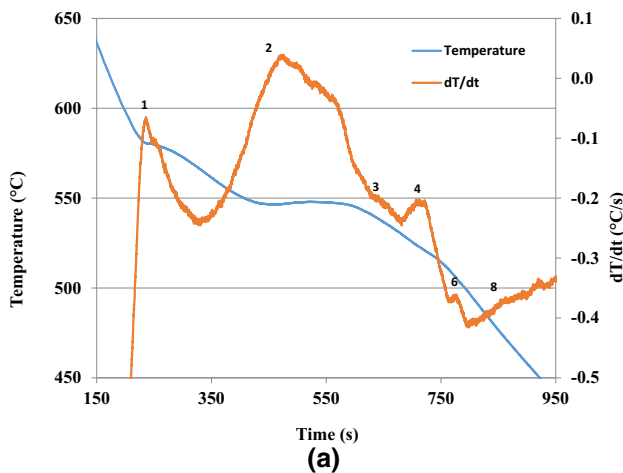


Figure 5. (a) Temperature–time plot and first derivative from the thermal analysis of alloy T (354 + 0.18%Zr + 3.6%Ni). (b) Optical microstructure of alloy T (354 + 0.18%Zr + 3.6%Ni) sample obtained from the corresponding thermal analysis casting (cooling rate 0.35 °C/s), showing the different phases present in the alloy: 1— AlCuNi ; 2— AlNiFe ; 3— AlTiZr ; 4— $\beta\text{-AlFeSi}$; 5— Al_2Cu .

Alloy S (354 + 0.21%Zr + 1.8%Ni)

The thermal analysis results for alloy S, i.e., 354 alloy containing 1.8 wt% Ni + 0.21 wt% Zr are plotted in Figure 4a. The presence of Ni results in the precipitation of Ni-containing phases, represented by the Reactions 3 and 6 as noted on the first derivative curve. In addition, due to the presence of Zr and Fe in Alloy S, another precipitate is formed, namely AlSiNiZrFe besides the AlFeNi phase.

The presence of the Q- $\text{Al}_5\text{Mg}_8\text{Cu}_2\text{Si}_6$ and Mg_2Si phases under the low solidification rate conditions of the thermal analysis experiment primarily depends on the Mg content. Although the Q-phase and Mg_2Si phase reactions were observed in the first derivative curve of alloy R, the proportion of Mg_2Si formed increased as the Mg level increased, as evidenced by Figure 4a and b in the case of Alloy S. It is also interesting to note from Figure 6 that, in alloy S, the Al_3CuNi phase is observed situated adjacent to the Al_2Cu phase and both phases are located at the limits of the dendritic α -Al phase. This observation is in agreement with the fact that the reactions noted in the thermal analysis curves, namely Reactions 6 and 7, appear consecutively.

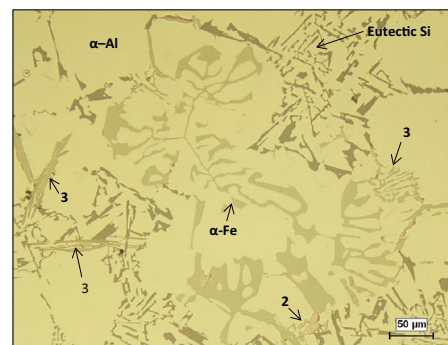
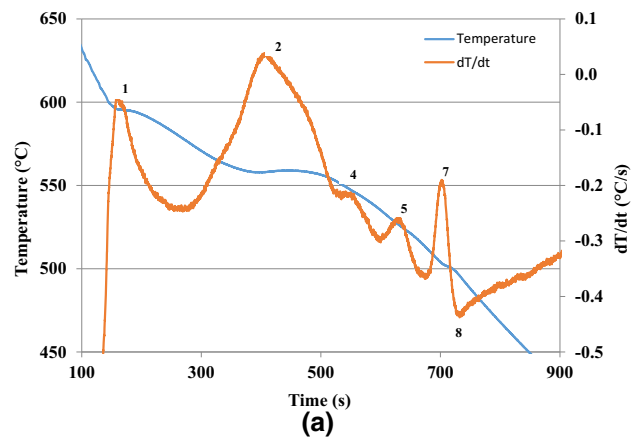


Figure 6. (a) Temperature–time plot and first derivative from the thermal analysis of alloy U (354 + 0.19%Zr + 0.71%Mn). (b) Optical microstructure of alloy U (354 + 0.19%Zr + 0.71%Mn) sample obtained from the thermal analysis casting (cooling rate 0.35 °C/s), showing the different phases present in the alloy: 2— Al_2Cu ; 3— AlSiMnFe .

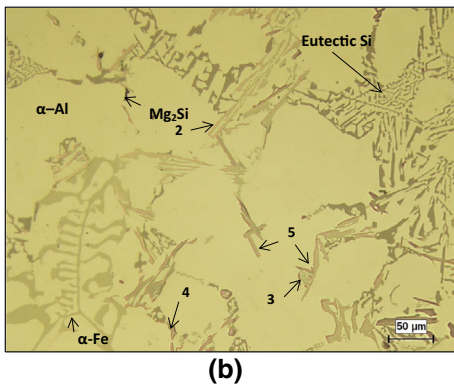
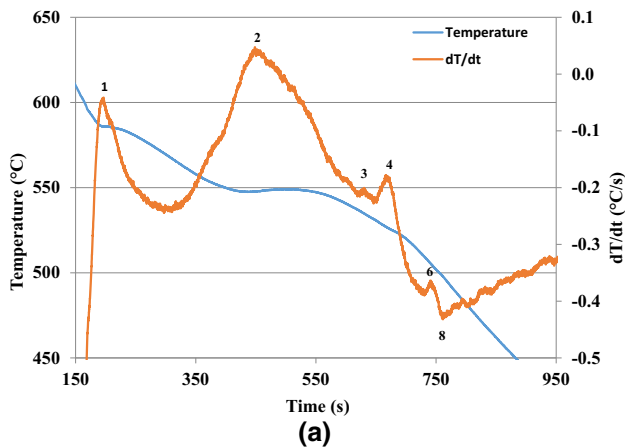


Figure 7. (a) Temperature–time plot and first derivative from the thermal analysis of alloy V (354 + 0.21%Zr + 0.68%Mn + 1.7%Ni). (b) Optical microstructure of alloy V (354 + 0.21%Zr + 0.68%Mn + 1.7%Ni) sample obtained from the thermal analysis casting (cooling rate 0.35 °C/s), showing the different phases present in the alloy: 2—AlNiCu; 3—AlFeNiCu; 4—Al₂Cu; 5—Zr-rich phase.

Alloy T (354 + 0.18%Zr + 3.6%Ni)

The solidification curve of Alloy T which, similar to alloy S, contains the same level of Zr but with a higher Ni content of 3.6 wt%, as obtained from its temperature–time data is shown in Figure 5 along with its first derivative plot. Apart from the α -Al dendrites and the eutectic Si particles observed in the interdendritic regions, other phases may also be observed in the optical micrograph of the corresponding thermal analysis sample of alloy T namely the Ni-containing AlFeNi and AlCuNi phases, as shown in Figure 5a. It is interesting to note the larger sizes of AlFeNi and AlCuNi phase particles observed in this case, when compared to those seen in Figure 5b for the S alloy sample with its lower Ni content of 1.8 wt%.

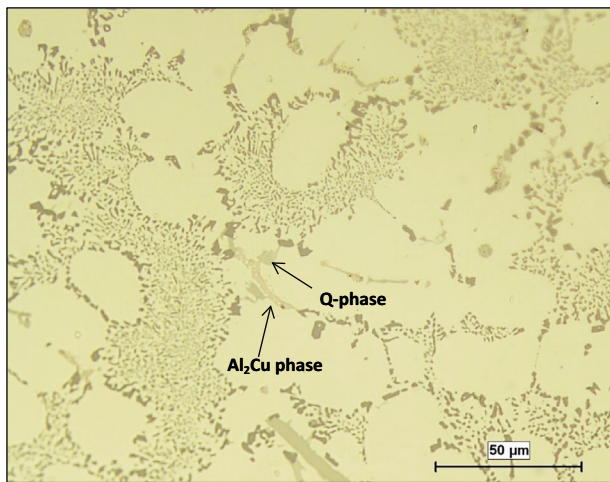
Alloy U (354 + 0.19%Zr + 0.71%Mn)

Figure 6a shows the solidification curve and its first derivative obtained for alloy U, namely 354 alloy containing 0.71 wt% Mn and 0.18 wt% Zr addition. The peaks 1, 2, 4, 5, 7 and 8 mark the reactions, which occur during solidification. As this alloy contains no Ni addition, Reactions 3 and 6 are not observed. It is interesting to note the broad width of peak #2 indicating that it encompasses other reactions besides the Al–Si eutectic reaction.

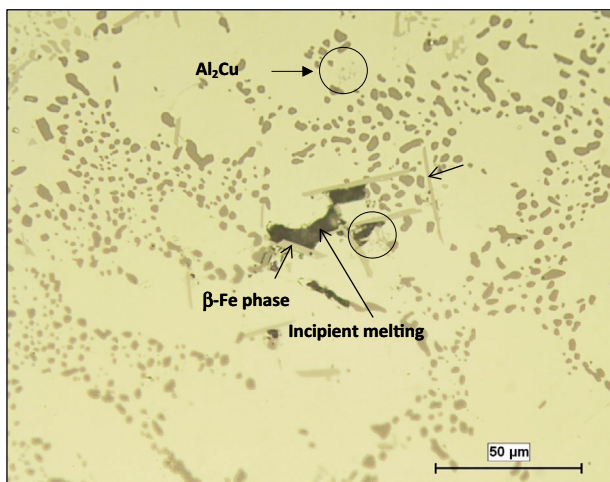
During solidification, iron, together with other alloying elements, partly goes into solid solution in the matrix and partly forms intermetallic compounds, including the platelet-like β -Al₅FeSi and the Chinese script-like α -Al₁₅(Mn,Fe)₃Si₂ phases. The latter is less detrimental to the

Table 4. Porosity Measurements for Alloys R, S, T, U and V

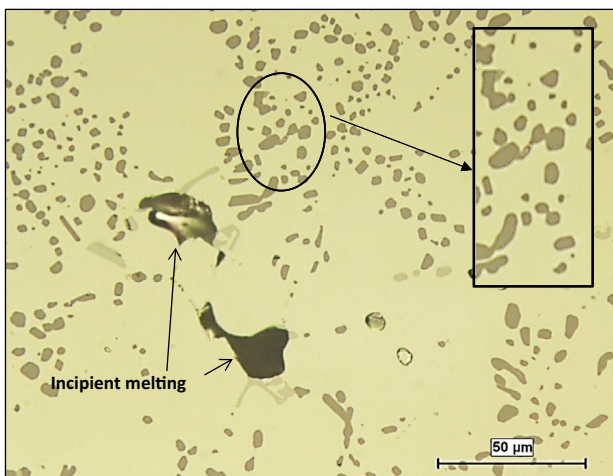
Alloy code	Condition	Area (%)		Pore area (μm^2)			
		Mean	SD	Mean	SD	SUM	Count
R	As cast	0.012	0.005	0.614	0.14	183	317
	SHT 1	0.063	0.018	4.45	4	1105.8	388
	SHT 2	0.067	0.035	12.45	7.36	1483.5	127
S	As cast	0.024	0.048	1.98	2.25	221.2	226
	SHT 1	0.075	0.032	8.98	7.38	1639.4	498
	SHT 2	0.087	0.038	3.5	2.88	1920.8	760
T	As cast	0.0082	0.006	2.13	1.76	180.1	79
	SHT 1	0.0629	0.0344	7.35	6.18	1378.1	268
	SHT 2	0.1	0.037	4.5	2.96	2214.2	693
U	As cast	0.02	0.021	2.08	8.35	441.2	212
	SHT 1	0.09	0.045	22	38.4	1959.2	89
	SHT 2	0.087	0.054	6.81	19.3	1913	281
V	As cast	0.011	0.011	1.16	2.61	238	206
	SHT 1	0.078	0.055	5.59	25.1	1710.9	306
	SHT 2	0.097	0.071	6.32	19.5	2130	337



(a) – R- As-cast



(b) – R-SHT 1



(c) – R-SHT 2

Figure 8. Optical micrographs of alloy R showing the microstructures observed in (a) as-cast, (b) SHT-1 and (c) SHT-2 tensile test samples (500x). Circled areas in (b) highlight dissolution of Cu-phases, whereas the inset at right in (c) reveals coarsening of Si particles observed in the circled area.

alloy properties than the β - Al_5FeSi phase because of its compact form, so that Mn is generally added to alloys containing Fe to “neutralize” the harmful effect of the β - Al_5FeSi intermetallic phase. If high iron and manganese levels are present in the alloy, and the cooling rate is low, the α - $\text{Al}_{15}(\text{Fe},\text{Mn})_3\text{Si}_2$ phase will precipitate as a primary phase, in the form of coarse particles termed “sludge,” having polygonal or star-like morphologies.

The optical micrograph of Figure 6b taken from the corresponding thermal analysis casting sample shows that the Mn addition in alloy U helps in reducing the detrimental effects of the β -iron phase by replacing it with the less-detrimental Chinese script α - $\text{Al}_{15}(\text{Fe},\text{Mn})_3\text{Si}_2$ phase and sludge particles. The precipitation of the α -Fe script phase within the α -Al dendrite actually strengthens the alloy matrix, as reported by Wang et al.¹⁸

Alloy V (354 + 0.21%Zr + 0.68%Mn + 1.7%Ni)

The solidification curve of alloy V which contains 0.68 wt% Mn and 0.21 wt% Zr additions similar to alloy U, but also 1.7 wt% Ni, obtained from its temperature–time data is shown together with its first derivative plot in Figure 7a. Apart from the α -Al dendrites and the eutectic Si particles observed in the interdendritic regions, other phases observed in the optical micrograph of the corresponding alloy sample are the α - $\text{Al}_{15}(\text{Fe},\text{Mn})_3\text{Si}_2$ script phase, the Ni-containing AlNi and AlCuNi phases, as well as small particles of Mg_2Si and the Al_2Cu phase, as shown in Figure 7b. Again, in this case also, the α -Fe script phase is observed to precipitate within the α -Al dendrite, indicating its primary nature.

Incipient Melting (Solidification Rate ~ 10 °C/s)

Solution heat treatment of tensile test bars is carried out to maximize the concentration of hardening elements such as Mg and Cu in solid solution, to homogenize the casting, and to alter the structure of the eutectic silicon particles in order to improve the mechanical properties. In Al–Si–Cu–Mg alloys, control of the solution treatment process is very critical because, if the solution heat treatment temperature exceeds the melting point, there is localized melting at the grain boundaries and the mechanical properties are reduced. In this study, the alloys were heat-treated using two different solution heat treatment processes: one-step and multi-step solution treatments. The multi-step solution heat treatment is carried out at three different temperatures consecutively, for different solution times, viz., 5 h at 495 °C, then 2 h at 515 °C, and then 2 h at 530 °C. A main consequence of incipient melting in Al–Si–Cu–Mg alloys is the melting of the Al_2Cu and Q-phases.

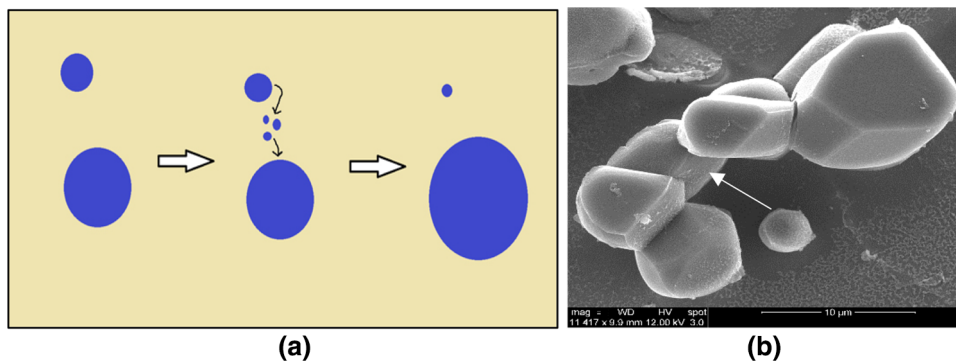


Figure 9. (a) Schematic showing coarsening of eutectic Si particles during solution heat treatment process²² and (b) coarsening of the eutectic Si particles during solutionizing treatment—note the presence of small particles in the vicinity of the large ones.

Samuel¹⁹ investigated incipient melting of $\text{Al}_5\text{Mg}_8\text{Si}_6\text{Cu}_2$ and Al_2Cu intermetallics in unmodified and strontium-modified Al–Si–Cu–Mg (319) alloys during solution heat treatment. The author concluded that incipient melting of $\text{Al}_5\text{Mg}_8\text{Si}_6\text{Cu}_2$ and Al_2Cu phases takes place when the high-magnesium version of 319 is solution treated at temperatures above 505 °C for sufficiently lengthy periods; this results in distortion of the test bars (i.e., casting) and deterioration of the alloy mechanical properties. As reported by de la Sablonnière and Samuel,²⁰ the Al_2Cu intermetallic may melt at 525 °C; thus, when the temperature of the multi-step solution heat treatment reaches 530 °C, or when local heating occurs at any point in the sample, it is expected that the Al_2Cu phase will melt, causing the formation of porosity and, in turn, a deterioration in the mechanical properties.¹²

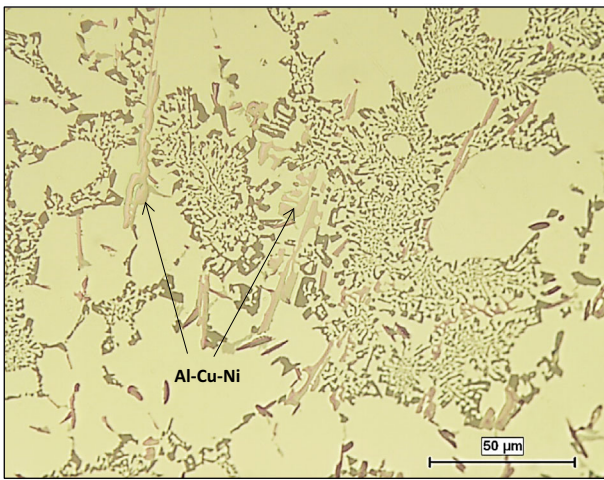
In the present study, all alloy melts were degassed to minimize the hydrogen level before casting. The only variable factor with respect to the cast samples would be the temperature, depending on the solution heat treatment conditions. Hence, any relatively significant changes in the porosity characteristics could be attributed to the melting of the copper phase(s) resulting from the changes in the temperature variable. Therefore, porosity measurements were carried out to monitor the incipient melting that resulted in the alloys studied, corresponding to the various solution heat treatments. The porosity characteristics resulting from incipient melting were examined and quantified using an optical microscope-Clemex Vision PE 4.0 image analysis system. Ten fields were examined for each alloy sample, at 200× magnification. The porosity parameters measured were the average area percent porosity (percentage porosity over a constant sample surface area), and the average pore area, total pore area (SUM) and the pore count. These values are listed in Table 4. As may be seen from Table 4, the as-cast sample for all alloys shows minimum porosity, whereas after solution heat treatment, the porosity values increase. In general,

compared to the one-step or SHT 1 treatment, the multi-step solution treatment leads to somewhat higher porosity values for the 354 alloys. This trend may be noted more clearly in the column showing the SUM or total area of the pores measured in each sample.

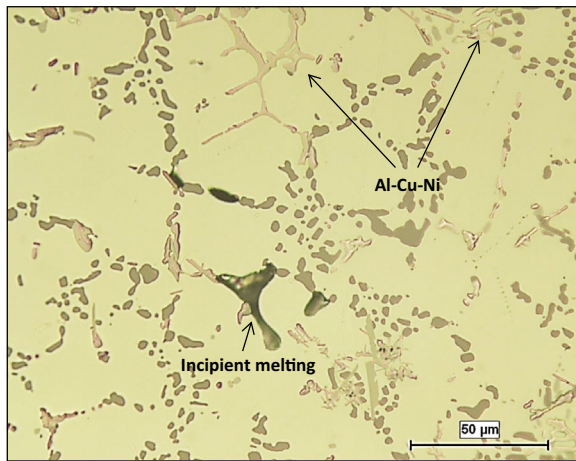
Figure 8a displays an optical micrograph of the as-cast alloy R sample, taken at 500× magnification, showing an overview of the sample surface, comprising the α -Al dendrites, modified eutectic Si regions, the β - Al_5FeSi phase as well as the Al_2Cu phase. Small particles of the π -Fe phase and the Q-copper phase are also seen. Upon solution heat treatment of the sample (one-step solution treatment), spheroidization of the Si particles is clearly noted and also some areas where incipient melting of the Al_2Cu phase has occurred, adjacent to β - Al_5FeSi phase platelets, as seen in Figure 8b. This is to be expected, since the eutectic Al_2Cu phase is generally observed to precipitate along the sides of the β -Fe platelets. Dissolution of the Cu-phases is also observed, as highlighted by the circled areas in Figure 8b. When the as-cast sample is subjected to the multi-step solution treatment—involving higher solution temperatures and longer durations, an increased amount of incipient melting is expected to occur, as may be noted in Figure 8c.

Coarsening of the Si particles is also observed, with larger particles growing bigger at the expense of smaller ones, in accordance with the Ostwald ripening phenomenon.^{21,22} A schematic representation of the coarsening process is shown in Figure 9a. The Ostwald ripening occurs through the dissolution of smaller Si particles, diffusion of the solute and re-precipitation onto larger particles. Thus, small particles decrease in size until they disappear and large particles grow larger. Figure 9b is an example observed in the present work showing the dissolution of the small Si to contribute to the size of the larger ones.

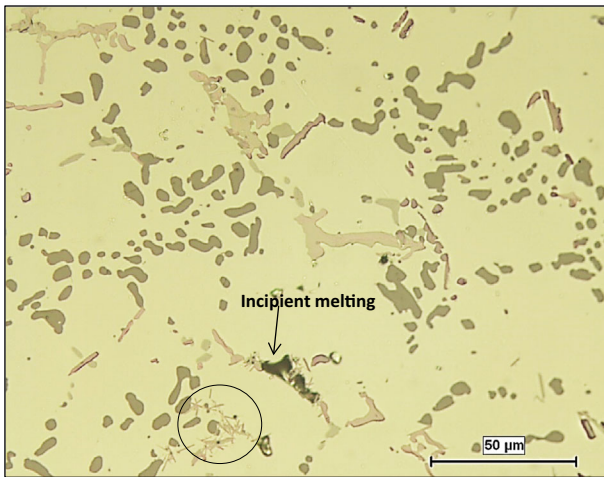
Compared to the base alloy R, in the case of alloy S which contains 0.23 wt% Zr + 1.8 wt% Ni, the as-cast



(a) – S-As-cast



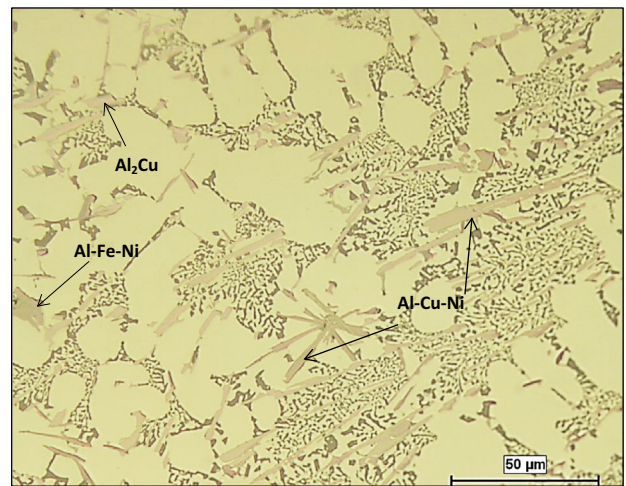
(b) – S-SHT 1



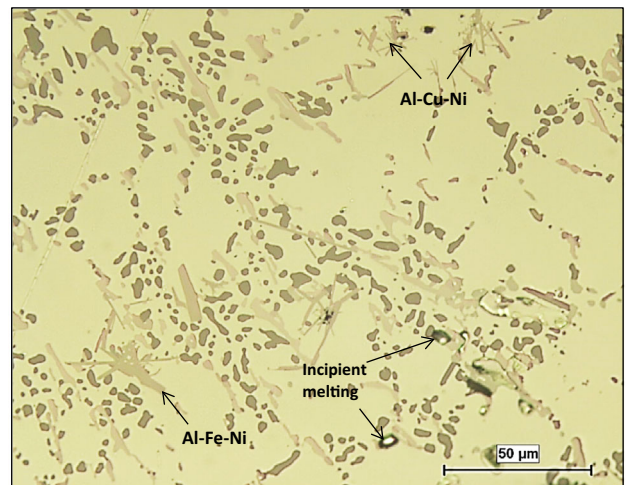
(c) – S-SHT 2

Figure 10. Optical micrographs of alloy S showing the microstructures observed in (a) as-cast, (b) SHT-1 and (c) SHT-2 tensile test samples (500×).

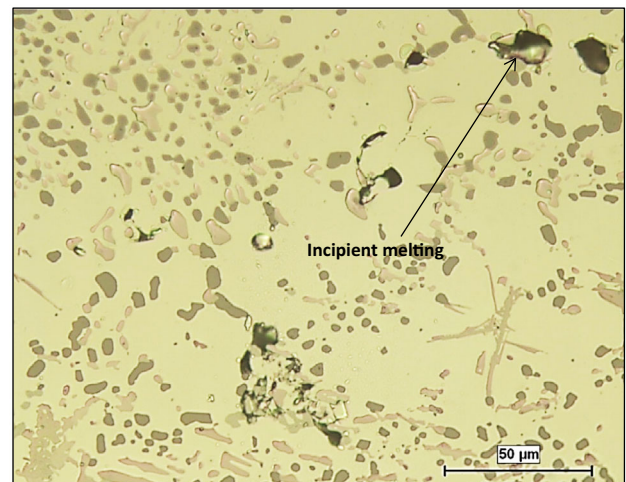
microstructure displays several Al–Cu–Ni particles, in script-like form, Figure 10a. After solution heat treatment, a certain amount of incipient melting is observed, as well as the dissolution of Cu-phase and Al–Cu–Ni particles, as



(a) – T-As-cast

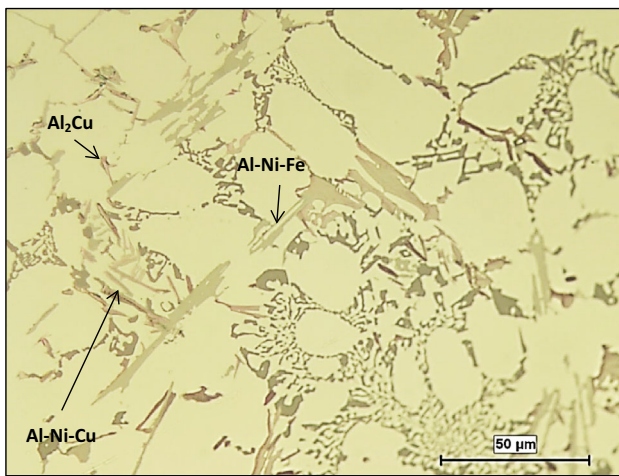


(b) – T-SHT 1

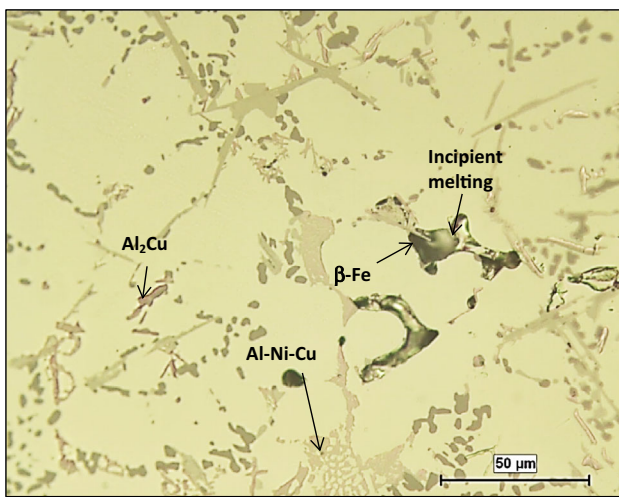


(c) – T-SHT 2

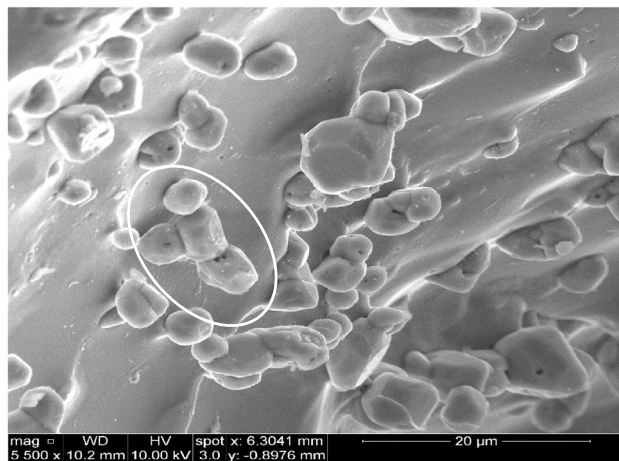
Figure 11. Optical micrographs of alloy T showing the microstructures observed in (a) as-cast, (b) SHT-1 and (c) SHT-2 tensile test samples (500×).



(a) – V-As-cast



(b) – V-SHT 1



(c) – V-SHT 2

Figure 12. Optical micrographs of alloy V showing the microstructures observed in (a) as-cast, (b) SHT-1 (500×) and (c) secondary electron image of SHT-2 tensile test sample (5500×)—note agglomeration of the Si particles within the melted zone.

evidenced, respectively, by the small-sized pink particles observed across the matrix and the smaller size of the Al–Cu–Ni particles in Figure 10b. In Figure 10c, very fine needles of Al–Cu–Ni observed in the circled area show the persistence of these Ni-containing particles even after long solution treatment times.

Figure 11 reveals the profusion of the Al–Cu–Ni phase in Alloy T, which persists even after solution treatment SHT-2.

Figure 12a and b exhibits the optical microstructures of as-cast and SHT-1 samples of alloy V. Examination of the pore area where incipient melting occurred in the solution treated sample revealed the presence of eutectic Si particles within the melted zone. As shown in the electron image of Figure 12c taken at 5500× magnification, revealing the agglomeration of the Si particles (white circled area) in the SHT-2 treated sample after the multi-step (prolonged) solution treatment.

Conclusions

Based on the microstructural results, thermal analysis data and porosity formation measurements, corresponding to the different 354 alloys containing Zr, Ni, Mn additions (viz., alloys R, S, T, U, V), the following conclusions may be drawn:

1. Six main reactions are detected during the solidification of the 354 base alloy:
 - (i) Formation of the α -Al dendritic network at 598 °C, followed by
 - (ii) precipitation of the Al–Si eutectic and the post-eutectic β -Al₅FeSi phase at 560 °C;
 - (iii) Mg₂Si phase formation at 540 °C;
 - (iv) transformation of the β -iron Al₅FeSi phase into π -Al₈Mg₃FeSi₆ phase at 525 °C; and
 - (v, vi) solidification of the copper-containing phases Al₂Cu and Q -Al₅Mg₈Cu₂Si₆ that solidify at 498 °C and 488 °C.
2. While minimum iron content is always recommended in the production of the 354 casting alloys, when such alloy castings contain high iron levels, appropriate solution heat treatment procedures may partially neutralize the deleterious effects of the iron-bearing phases.
3. As a result of the low solidification rate of the thermal analysis castings, all Zr-containing alloys are located in the L + Al₃Zr region of the Al–Zr phase diagram during solidification and form primary AlZr particles.
4. Three main reactions are detected with the addition of Ni, i.e., the formation of AlFeNi, AlCuNi and AlSiNiZr phases.

5. Larger sizes of AlFeNi and AlCuNi phase particles are observed in the T alloy with a Ni content of 3.6 wt%, when compared to those seen in the S alloy sample with its lower Ni content of 1.7 wt%.
6. Mn addition in Alloy U helps in reducing the detrimental effects of the platelet morphology of the β -iron Al₅FeSi phase by replacing it with the more compact and hence less-detrimental Chinese script α -Al₁₅(Fe,Mn)₃Si₂ phase and sludge particles.

Acknowledgements

The authors would like to thank Amal Samuel for enhancing the quality of the images used in the present article.

REFERENCES

1. J. Hernandez-Sandoval, G.H. Garza-Elizondo, A.M. Samuel, S. Valtierra, F.H. Samuel, The ambient and high temperature deformation behavior of Al–Si–Cu–Mg alloy with minor Ti, Zr, Ni additions. *Mater. Des.* **58**, 89–101 (2014)
2. A.M.A.Mohamed, F.H. Samuel and A.M. Samuel, Effect of Fe, Mn, Cu and Mg additions on the mechanical properties of Al-10.8 wt% Si near-eutectic alloy, in *18th Canadian Materials Science Conference* (McGill University, Montreal, QC, Canada, 2006)
3. Z. Jia, G. Hu, B. Forbord, J.K. Solberg, Effect of homogenization and alloying elements on recrystallization resistance of Al–Zr–Mn alloys. *Mater. Sci. Eng., A* **444**(1), 284–290 (2007)
4. A.J. Tolley, V. Radmilovic, U. Dahmen, On the effect of Zr on precipitate evolution in Al–Sc–Zr alloys, in *Congress CONAMET/SAM 2004 Proceedings* (La Serena, Chile, 2004)
5. F. Stadler, H. Antrekowitsch, W. Fragner, H. Kaufmann, P.J. Uggowitzner, The effect of Ni on the high-temperature strength of Al–Si cast alloys, in *Materials Science Forum*, Vol. 690. (Trans Tech Publications, 2011). pp. 274–277
6. Y.H. Cho, D.H. Joo, C.H. Kim, H.C. Lee, The effect of alloy addition on the high temperature properties of over-aged Al–Si (CuNiMg) cast alloys, in *Materials Science Forum*, Vol. 519. (Trans Tech Publications, 2006). pp. 461–466
7. V.G. Davydov, T.D. Rostova, V.V. Zakharov, Y.A. Filatov, V.I. Yelagin, Scientific principles of making an alloying addition of scandium to aluminium alloys. *Mater. Sci. Eng., A* **280**(1), 30–36 (2000)
8. K.E. Knippling, D.N. Seidman, D.C. Dunand, Ambient- and high-temperature mechanical properties of isochronally aged Al–0.06 Sc, Al–0.06 Zr and Al–0.06 Sc–0.06 Zr (at.%) alloys. *Acta Mater.* **59**(3), 943–954 (2011)
9. Y. Harada, D.C. Dunand, Microstructure of Al₃Sc with ternary transition-metal additions. *Mater. Sci. Eng., A* **329**, 686–695 (2002)
10. M. Zeren, E. Karakulak, Influence of Ti addition on the microstructure and hardness properties of near-eutectic Al–Si alloys. *J. Alloys Compd.* **450**(1), 255–259 (2008)
11. G.K. Sigworth, T.A. Kuhn, Grain refinement of aluminum casting alloys. *Int. J. Metalcast.* **1**(1), 31–40 (2007)
12. L. Alyaldin, *Effects of Alloying Elements on Room and High Temperature Tensile Properties of Al–Si–Cu–Mg Base Alloys*. Master of Engineering Thesis, Université du Québec à Chicoutimi, Quebec, Canada 2017
13. G.H. Garza-Elizondo, A.M. Samuel, S. Valtierra, F.H. Samuel, Effect of transition metals on the tensile properties of 354 alloy: role of precipitation hardening. *Int. J. Metalcast.* **11**(3), 413–427 (2017)
14. L. Backerud, G. Chai, J. Tamminen, Solidification characteristics of aluminum alloys, in *Foundry Alloys*, vol 2 (American Foundrymen’s Society, Inc., 1990), p. 266
15. F.H. Samuel, A.M. Samuel, H.W. Doty, Factors controlling the type and morphology of Cu-containing phases in 319 Al alloys. *AFS Trans.* **104**, 893–901 (1996)
16. A.M. Nabawy, *Influence of Zirconium and Scandium on the Microstructure, Tensile Properties, and Hot-Tearing Susceptibility of Al–2 wt%Cu-Based Alloys*. PhD Thesis, Université du Québec à Chicoutimi, Chicoutimi, Quebec, Canada, 2010
17. D. Srinivasan, K. Chattopadhyay, Non-equilibrium transformations involving, L1₂–Al₃Zr in Ternary Al–X–Zr alloys. *Metall. Mater. Trans. A* **36A**, 311–320 (2005)
18. E.R. Wang, X.D. Hui, G.L. Chen, Eutectic Al–Si–Cu–Fe–Mn alloys with enhanced mechanical properties at room and elevated temperature. *Mater. Des.* **32**(8), 4333–4340 (2011)
19. F.H. Samuel, Incipient melting of Al₅Mg₈Si₆Cu₂ and Al₂Cu intermetallics in unmodified and strontium-modified Al–Si–Cu–Mg (319) alloys during solution heat treatment. *J. Mater. Sci.* **33**(9), 2283–2297 (1998)
20. H. De la Sablonnière, F.H. Samuel, Solution heat treatment of 319 aluminum alloy containing ~ 0.5 wt%Mg. Part 2—microstructure and fractography. *Int. J. Cast Met. Res.* **9**(4), 213–225 (1996)
21. A.S. Kabalnov, A.V. Pertsov, E.D. Shchukin, Ostwald ripening in two-component disperse phase systems: application to emulsion stability. *Coll. Surf.* **24**, 19–32 (1987)
22. A. Kabalnov, Ostwald ripening and related phenomena. *J. Dispers. Sci. Technol.* **22**, 1–12 (2001)

Publisher’s Note Springer Nature remains neutral with regard to jurisdictional claims in published maps and institutional affiliations.